ARTICLES

Symmetry considerations regarding light propagation and light polarization for coherent interactions with ions in crystals

Y. Sun, G. M. Wang, and R. L. Cone
Department of Physics, Montana State University, Bozeman, Montana 59717

R. W. Equall
Scientific Materials Corporation, Bozeman, Montana 59715

M. J. M. Leask
Clarendon Laboratory, Parks Road, Oxford OX1 3PU, United Kingdom
(Received 30 August 2000)

Spectroscopic studies and the efficiency of optical coherent transient devices can be adversely affected by interference arising from several distinct Rabi frequencies associated with crystallographically equivalent but orientationally inequivalent crystal sites. General symmetry principles have been used to find light field directions that guarantee both optimum single-Rabi-frequency interaction and the most efficient coherent transient generation in arbitrary crystals. This theoretical analysis has been applied experimentally to a wide range of rare earth crystals, many of which are important for technological applications. Site interference in optical nutation provides a simple illustration of this effect. Optimum single-Rabi-frequency nutation signal was obtained for the $^3H_6(1)$ to $^3H_4(1)$ transition of 0.1% $Tm^{3+}:Y_3Al_5O_{12}$ when the light $\vec{E}$ vector is along special crystal directions $\langle 111\rangle$ or $\langle 001\rangle$. Quantitative comparison of nutation frequencies for light polarized along different directions allowed the determination of the optical transition dipole moment to be along $\langle 110\rangle$ for this transition. The transition dipole moment derived from the nutation signal agrees within 15% with that obtained from absorption experiments. Other applications of nutation measurements are discussed, including a procedure for determining site occupancy in crystals with crystallographically inequivalent sites.

I. INTRODUCTION

A variety of optical-electronic applications and spectroscopic techniques are based on the coherent interaction of optical radiation fields with ion-doped or molecular crystals of various types; these interactions include optical coherent transients, spectral hole burning, and spatial-spectral holography or time- and space-domain holography.[1–4] Devices based on coherent transient concepts are useful in optical data storage, real-time optical signal processing, and optical data routing and have applications including computers, communications networks, the internet and other networks, optical correlators, true time delays in radar, and numerous other applications.

In this paper, we are concerned with optimizing the generated optical coherent transient signals. For reasons explained in the next paragraph, coherent signals with several time dependences are typically generated, and the interference of these signals reduces the sensitivity and effectiveness of the spectroscopic technique and the efficiency and time resolution in device applications. All possible combinations of space and point groups have been examined, and combinations of light polarization and propagation directions have been identified that result in a simplified *single-Rabi-frequency* temporal behavior. That is, for these special identified single-Rabi-frequency directions, all active ions in the crystal will be driven in phase, and this provides a much simpler coupling between the ions and the radiation field and a cleaner transient response.

Natural and synthetic optical materials have a wide range of potential crystal lattice symmetries.[5] Within these materials, active ions or molecules occupy crystal lattice sites that can be cataloged into subsets, with members of each subset having identical surroundings and having the same resonant frequency for coupling to optical radiation; the members of each subset are said to be crystallographically equivalent. Each crystallographically equivalent subset of lattice sites, however, may contain ions or molecules with a finite number of different spatial orientations, and these may be described as orientationally inequivalent. The optical transitions of the ions or molecules can be described by two energy levels and a transition dipole moment. In general, these transition dipole moments can have different spatial orientations, according to the different orientations of the crystallographically equivalent but orientationally inequivalent sites noted above. Polarized light beams, with a single optical propagation direction, can have many different spatial relationships with otherwise identical ions or molecules. When resonant coherent interactions occur, the interaction of the optical field and the two-level systems can be characterized by the optical Rabi frequency $\Omega = \vec{p} \cdot \vec{E}_0 / \hbar$, where $\vec{p}$ is the electric dipole

moment with components $p_i=\langle 1|p_i|2\rangle$ and $\vec{E}_0$ is the optical electric field vector.[6] Similar expressions apply for magnetic dipoles and magnetic optical fields. The Rabi frequency is determined not only by the magnitudes of the transition dipole moment and of the optical field, but also by the projection of one onto the other. Consequently, when arbitrarily polarized radiation is propagated through such materials with transition dipoles pointing in different directions, the coherent interaction of the field and the crystalline matter will induce macroscopic polarization oscillations at several different optical Rabi frequencies rather than giving the desired single-Rabi-frequency response. In device applications, the presence of multiple optical Rabi frequencies generally reduces the effectiveness due both to consequent complex transient material polarization behavior and to reduction of the associated optical signal amplitudes radiated by the material. Such interference can in turn limit the optical-electronic system bandwidth and hence the response time and data handling capability. The interference may also reduce the optical diffraction efficiency, i.e., the signal selection or deflection efficiency in such devices as optical data routers[7] for optical communications networks and wavelength-division multiplexing systems. In fundamental studies of material properties, the confusing optical beating complicates determination of transition dipole moments and comparison of various transitions. Here we show that both fundamental studies and device applications benefit from specific choices of light polarization relative to the crystal lattice structure.

To avoid the deleterious effects of this multiple-frequency interference, while still being able to optimize other system parameters, it is necessary to be able to obtain single-Rabi-frequency behavior through a choice of experimental conditions. The small group of materials that have only a single site orientation can readily exhibit single-Rabi-frequency behavior. Here, we show that any low-symmetry material also can exhibit single-Rabi-frequency behavior. To be able to use a low-symmetry material that has otherwise ideal properties in these applications will be a great advantage.

We consider, in this paper, the dynamics of two-level systems under coherent excitation that involves orientational inequivalence, i.e., the transitions correspond to the same crystallographic site and have the same transition frequency, but the transition dipoles are oriented differently in the crystal. Specifically, we study the interference effect of these dipoles in optical nutation and provide special light polarization directions onto which all active transition dipoles project identically. In some materials this is relatively simple and may be achieved for all active ions. For the remaining class of materials, it is possible to achieve the simple single-Rabi-frequency behavior for only a subset of ions, but it is still possible to achieve the desired behavior by simultaneously turning off coupling to the remaining group(s) of active ions. In summary, single-Rabi-frequency behavior can be achieved for all crystal classes either by making all dipoles project along the optical field in the same way or by making some of them project the same while others are perpendicular to the light field and do not participate in the transition.

To illustrate one of our solutions, optical nutation was used to directly measure the Rabi frequency. Optical nutation was chosen as a simple prototype for a broad range of optical coherent transients, and similar advantages are obviously gained in those other cases. Optical nutation was first observed experimentally by Hocker and Tang in 1968.[8] Brewer and co-workers developed Stark switching and frequency switching techniques[9,10] for observing a number of transient phenomena including optical nutation, free induction decay, photon echoes, and others. Interference effects in these transient phenomena, caused by the simultaneous excitation of many levels, have been observed. The interaction of an atomic system with magnetic sublevel degeneracy with coherent light has been described theoretically by Shore[11] and a demonstration of this effect was given by Delsart and Keller[12] and later by Kastberg *et al.*[13] Here we demonstrate the interference effect due to orientational inequivalence of the transition from contributions of multiple differently oriented sites.

The direct measurement of the Rabi frequency, and thus the pulse area in a transient experiment, provides a way of measuring the oscillator strength of an optical transition, independent of an absorption experiment.[14] Interpretation of absorption experiments requires the number density of active ions, and that often cannot be known accurately. In some crystals, there might be multiple crystallographically inequivalent sites for the same ion, and there is no easy way to know the percentage of dopant ions in each site beforehand. Optical nutation provides an independent way of measuring the oscillator strength and allows determination of site occupancy. For example, we have measured the optical nutation on the ${}^3H_4$-${}^1D_2$ transition in Pr^{3+}:Y_2SiO_5 for Pr^{3+} ions in both Y^{3+} lattice sites. Combining the nutation experiment with an absorption experiment has allowed us to show that the two crystallographic sites have very different (more than ten times different) occupancy by the Pr^{3+} ions, probably due to the large ionic radius mismatch between Pr^{3+} and Y^{3+} and the specific site properties in the crystal. Details of that experiment will be discussed in a subsequent paper.[15]

In many systems, the direction of the transition dipole may not be known relative to the local axes, and it is not easy to measure traditionally. Optical nutation provides a simple way to find this direction, as we show here for the ${}^3H_6(1)\leftrightarrow{}^3H_4(1)$ transition in Tm^{3+}:$Y_3Al_5O_{12}$ (YAG).

We first give a simple introduction to nutation theory and the functional form for the nutation signal in the ideal situation of a Gaussian beam. In systems with multiple site orientations, the nutation signal arises from a sum over all the sites with different Rabi frequencies. We then describe a procedure for finding the symmetry direction for light polarization in an arbitrary crystal, so that there will be only one Rabi frequency. The results for all combinations of space groups and point groups have been tabulated. The derived behavior has been observed in a wide range of rare earth crystal systems. As an illustration, we present our optical nutation experiment on the ${}^3H_6(1)\leftrightarrow{}^3H_4(1)$ transition of 0.1% Tm^{3+}:$Y_3Al_5O_{12}$, where we have varied the light polarization in the crystal and measured the optical nutation with six interfering Rabi frequencies. In the discussion of this experiment, we show that all of the nutation signals for completely arbitrary polarizations can be simulated by multiple site interference, and when the polarization is aligned along the predicted symmetry directions single-Rabi-frequency behavior results. From these measurements, we

also have determined the direction of the transition dipole moment.

II. NUTATION THEORY

A two-level system driven by a resonant, monochromatic field exhibits optical nutation as the ions are coherently driven between the ground and excited states. The nutation frequency exactly on resonance is $\Omega=\vec{p}\cdot\vec{E}_0/\hbar$, where $\vec{p}$ is the transition dipole moment and $\vec{E}_0$ is the amplitude of the electric field. For off-resonance ions, the nutation frequency is given by $(\Delta^2+\Omega^2)^{1/2}$ where Δ is the detuning. Due to the presence of inhomogeneous broadening, the nutation takes the form of $\Omega^2 J_0(\Omega t)$ from the averaging effect of all ions under the inhomogeneous line shape, even with monochromatic excitation.[16] In an experiment using a Gaussian beam, averaging over the whole transverse beam profile makes the nutation behave as $\Omega^2 J_1(\Omega t)/\Omega t$, so that the ''Rabi frequency'' of the nutation is still determined by the intensity in the center of the beam. The phase relaxation of the system and spontaneous emission make it impossible for an analytical form of the nutation to be obtained, but we can take into account the inhomogeneous dephasing of the system by writing

$$e^{-t/T_2^*}\Omega^2\frac{J_1(\Omega t)}{\Omega t}, \tag{1}$$

where T_2^* is an inhomogeneous dephasing time determined by material coherence properties and laser excitation bandwidth. In an experiment with high optical density, the averaging effect along the optical path in the sample can also alter the nutation pattern since the light intensity decreases along the path. Depending on the relative amplitudes of T_2^* and $1/\Omega$, we may or may not be able to observe the nutation signal. That problem did not arise in the experiments described here.

In a crystalline system with many crystallographic sites, transition dipoles for the same optical transition frequency can have different spatial orientations. These different sites usually have different nutation frequencies ($\Omega_i=\vec{p}_i\cdot\vec{E}_0$) due to the different projections of $\vec{E}_0$ along the local dipoles on orientationally inequivalent sites. The total nutation signal can be expressed as the addition of the original electric field and the polarizations of all the sites. A first-order approximation assuming small material polarization (compared to the external field intensity) gives the intensity of the nutation signal as

$$I\propto \text{const}+\sum_i\ (\Omega_i)^2\frac{J_1(\Omega_i t)}{\Omega_i t}e^{-t/T_2^*}. \tag{2}$$

The resulting signal normally has a complicated irregular temporal shape. Similar effects have been observed in atomic beam systems with magnetic substate degeneracy.[11,13]

III. GENERAL SOLUTION FOR SINGLE-RABI-FREQUENCY BEHAVIOR

The interference of the different terms in Eq. (2) will be constructive, giving a nutation signal with maximum amplitude and a simple wave form when all Rabi frequencies Ω_i are the same. Since the nutation frequency for an individual ion is determined by the scalar product of its transition dipole moment and the electrical field vector $\vec{E}_0$ of the light, this requirement can be met by choosing an $\vec{E}_0$ such that all excited dipoles project identically onto it.

Through exhaustive consideration of all possible combinations of the 32 point groups and the 230 space groups,[5] we have shown that a solution exists for all physically allowed combinations. For uniaxial crystals, this $\vec{E}_0$ direction can be chosen to be the unique axis. For biaxial crystals it can be chosen to be the optical normal, although other directions may also serve this purpose, especially if the transition dipole is perpendicular to the above mentioned direction. For an arbitrary crystal symmetry, the general procedure described below has been developed for finding a suitable direction. First, one finds a light polarization direction $\vec{E}_0$ with equal projections on a subset n of the m different local dipole directions ($n\leqslant m$). This direction has to be perpendicular to the remaining $(m-n)$ dipoles. Second, one propagates the light beam perpendicular to the polarization direction chosen. While it may not be obvious that this is possible for all cases, we have considered each in turn and have tabulated the results of this analysis in Table I for linearly polarized light. For limited combinations of space and point groups, special characters of circularly polarized transitions can also be considered. Circularly polarized transitions can occur only in uniaxial or cubic crystals. For those cases, the transition dipole can be thought of as rotating *around* a particular axis, left or right handed. In uniaxial crystals, that axis can only be the unique optical axis, and circularly polarized light with proper handedness should be propagated along this axis to achieve a single Rabi frequency. In cubic crystals, the axis can only be along the $\langle 100\rangle$ and/or $\langle 111\rangle$ axes. If the axis is along $\langle 100\rangle$, circularly polarized light with proper handedness propagating along any of the $\langle 100\rangle$ axes induces a single Rabi frequency. For the specialized case of the axis along $\langle 111\rangle$, no single-Rabi-frequency direction can be found to propagate the light due to the nonorthogonality of these axes.

In Table I, at least one solution is listed for all possible combinations of crystal host systems (space groups) and local crystal sites (point groups). For a small fraction of the cases, with a combination of high crystal symmetry and very low site symmetry, a solution exists only when the transition dipoles are aligned along some specific directions in the crystal. For example, at the end of Table I, we have listed the combination of crystal systems with O_h symmetry and local sites with C_1 symmetry. A single dipole direction can be found only when the dipoles are aligned along C_4 or C_2'; a general solution is not available when the dipoles are along an arbitrary direction.

For birefringent crystals, considerations were limited to the major polarization axes and planes. Other arbitrary polarizations were not considered because the change in polarization state during propagation would invalidate such choices.

The rare-earth-doped crystals that have been used in all demonstrations of coherent transient applications have general solutions. We have experimentally tested the cases of

TABLE I. All the single-Rabi-frequency directions for all crystal symmetries and for every possible site symmetry for each crystal symmetry. When there are several possibilities for the same symmetry label, the labels C_2' and C_2'' were also used in addition to C_2, and σ_d, σ_v are used for the vertical mirror planes in the convention of Koster *et al.* (Ref. 27).

Crystal classes	Possible site symmetries	Conditions	Single-Rabi-frequency directions
		Triclinic	
C_1	C_1		all (all directions work)
C_i	C_i		all
	C_1		all
		Monoclinic	
C_2	C_2		all
	C_1		$\parallel$ and $\perp C_2$ and a plane that bisects the dipoles
$C_s(C_{1h})$	C_1		$\parallel\sigma$ and $\perp\sigma$
	C_s		all
C_{2h}	C_1, C_i, C_s		$\sigma_h, \parallel C_2$
	C_2, C_{2h}		all
		Orthorhombic	
D_2	C_1, C_2		3 C_2's
	D_2		all
C_{2v}	C_1, C_2, C_s		3 C_2's
	C_{2v}		all
D_{2h}	$C_1, C_2, C_s, C_i, C_{2h}$		3 C_2's
	C_{2v}, D_2, D_{2h}		all
		Tetragonal	
C_4	C_1, C_2		$\parallel C_4$, 4 directions $\perp C_4$ and 45° from each other
	C_4		all
S_4	C_1, C_2		$\parallel S_4$, 4 directions $\perp C_4$ and 45° from each other
	S_4		all
C_{4h}	C_1, C_2, C_s, C_{2h}		$\parallel C_4$, 4 directions $\perp C_4$ and 45° from each other
	C_4, S_4, C_{4h}		all
D_4	C_1, C_2		C_4 axis
	D_2, C_2', C_2''		C_4, C_2', C_2''
	C_4, D_4		all
C_{4v}	C_1, C_2		C_4 axis
	C_{2v}, C_s		C_4 axis and $\perp C_4$ in σ_d and σ_v
	C_4, C_{4v}		all
D_{2d}	C_1, C_2		S_4 axis
	D_2, C_{2v}, C_s, C_2'		S_4, C_2' axes and 2 directions $\perp S_4$ in σ_d
	S_4, D_{2d}		all
D_{4h}	C_1, C_2, C_i, C_s		C_4 axis
	$D_2, C_{2h}, C_{2v}, C_2', C_2'',$ $C_s'(\sigma_d, \sigma_v)$		C_4, C_2', C_2''
	$S_4, C_4, C_{4h}, D_4, C_{4v}, D_{2d}, D_{4h}$		all
		Trigonal	
C_3	C_1		$\parallel C_3$ and 3 directions $\perp C_3$ (120° apart)
	C_3		all
C_{3i}	C_1, C_i		$\parallel C_3$ and 3 directions $\perp C_3$ (120° apart)
	C_3, C_{3i}		all
D_3	C_1		$\parallel C_3$
	C_2	if $\parallel C_2$	$\perp$ to both C_2 and C_3
		if $\perp C_2$	C_2 and C_3 axes
	C_3, D_3		all
C_{3v}	C_1		$\parallel C_3$
	C_s	if $\perp\sigma_v$	3 direction $\perp C_3$ in σ_v
		if in σ_v	C_3 and $\perp\sigma_v(3)$
	C_3, C_{3v}		all

TABLE I. (*Continued*).

Crystal classes	Possible site symmetries	Conditions	Single-Rabi-frequency directions
D_{3d}	C_1		C_3 axis
	C_2, C_{2h}, C_s	if $\|C_2$	$\perp$ to C_3 in the mirror planes
		if $\perp C_2$	C_3 axis and 3 directions along C_2
	D_3, C_{3v}, D_{3d}		all
		Hexagonal	
C_6	C_3, C_6		all
	C_1, C_2		C_6 axis, and 3 directions $\perp$ to C_6
C_{3h}	C_3, C_{3h}		all
	C_1, C_s		C_3 axis, and 3 directions $\perp$ to C_3
C_{6h}	C_6, C_{3h}, C_3, C_{6h}, C_{3i}		all
	C_1, C_i, C_2, C_s, C_{2h}		C_6 axis, and 3 directions $\perp$ to C_6
D_{3h}	C_3, C_{3h}, C_{3v}, D_3, D_{3h}		all
	C_{2v}, C_2, C_s		C_3 and 3 C_2's or C_3 and 3 directions $\perp$ to C_2 and C_3
	C_1		C_3 axis
C_{6v}	C_3, C_{3v}, C_6, C_{6v}		all
	C_{2v}, $C_s'(\sigma_d,\sigma_v)$		C_6 and $\perp\sigma_d$, or $\perp\sigma_v$
	C_1, C_2		C_6 axis
D_6	C_3, D_3, D_6		all
	D_2, C_2', C_2''		C_6 axis and C_2' or C_2''
	C_1, C_2		C_6
D_{6h}	C_3, Cv, C_{3h}, C_{3i}, D_3, C_6,		all
	D_{3h}, D_{3d}, C_{6v}, C_{6h}, D_6		
	D_2, D_{2h}, C_{2v}, C_2', C_2'',		C_6 and C_2' or C_2''
	C_{2h} (C_2 axis of $C_{2h} \perp C_6$ axis) $C_s'(\sigma_d,\sigma_v)$		
	C_1, C_i, C_s, C_2, C_{2h}		C_6 axis
		Cubic	
T	C_1, C_2	if $\|C_2$	C_2 and C_3 axes
	C_3		C_2 axes
	D_2		C_3 and C_2 axes
	T		all
T_h	T, T_h		all
	C_3, C_{3i}		C_2
	D_{2h}, D_2, C_{2v}		C_2 and C_3
	C_1, C_i, C_s, C_2, C_{2h}	if $\|C_2$	C_2, C_3 and $\perp C_2$ in mirror plane
T_d	T,T_d		all
	C_3,C_{3v}		S_4
	D_{2d}, S_4		S_4, C_3, and $\perp$ S_4 in mirror plane
	D_2,C_{2v}		S_4,C_3
	C_1, C_2, C_s	If $\|S_4$	S_4,C_3
		or $\perp\sigma_d$	
O	T,O		all
	C_3, D_3		C_4
	D_4, C_4		C_4,C_3, C_2'
	D_2		C_4,C_3
	C_1, C_2	if $\|C_4$	C_4,C_3,C_2'
		if $\|C_2'$	C_4,C_3
O_h	T, T_h, T_d, O, O_h		all
	C_3,C_{3i},C_{3v},D_3,D_{3d}		C_4
	D_4, C_{4v}, D_{2d}, D_{4h}, C_4, S_4, C_{4h}		C_4 and C_3 and C_2'
	D_2, C_{2v}, D_{2h}		C_4 and C_3
	C_1, C_2, C_s, C_i, C_{2h}	if $\|C_4$	C_4 and C_3 and C_2'
		if $\|C_2'$	C_4 and C_3

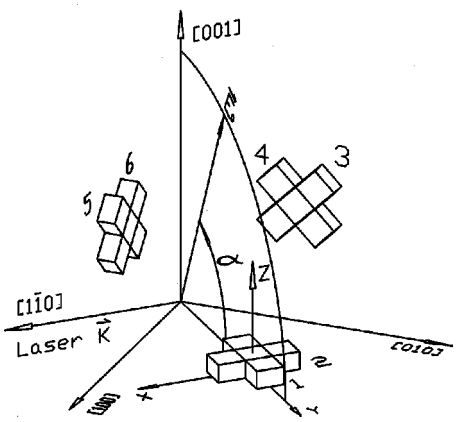

FIG. 1. Orientations of the six orientationally inequivalent sites of the Y^{3+} ion in the yttrium aluminum garnet crystal lattice (Ref. 26). Each lozenge-shaped parallelepiped represents the local D_2 symmetry for a subset of sites. The x, y, and z axes are the local axes for site 1. Experiments were carried out with the light passing along the $[1\bar{1}0]$ axis and the light polarization was rotated from [110] to [001]. α is the angle between $\vec{E}_0$ and [110].

Pr^{3+}:Y_2SiO_5, Tm^{3+}:YAG, the Er^{3+} $^4I_{15/2}(1) \leftrightarrow {}^4I_{13/2}(1)$ transition in Er^{3+}:$YAlO_3$, Er^{3+}:$LiNbO_3$, Er^{3+}:$CaWO_4$, Er^{3+}:$SrWO_4$, Er^{3+}:Y_2O_3, Er^{3+}:$Y_3Al_5O_{12}$, and Er^{3+}:Y_2SiO_5. Single-Rabi-frequency directions have been confirmed for each of them. Here we present optical nutation measurements for Tm^{3+}:YAG as an illustration of the broader range of results.

IV. EXPERIMENT

To illustrate the collective oscillation and the interference of the oscillations of all the sites in a crystal, we chose a two-level system: the $^3H_4(1)$ to $^3H_6(1)$ electronic transition of 0.1% Tm^{3+}:$Y_3Al_5O_{12}$. This transition occurs at 793.156 nm and is electric dipole allowed. This system has been studied spectroscopically[17–19] and used for the demonstration of several applications utilizing coherent transient techniques.[20–23] The excited state $^3H_4(1)$ has a long spontaneous decay time ($T_1 \sim 800$ μs) and a long dephasing time ($T_2 \sim 110$ μs) at 1.4 K. The $Y_3Al_5O_{12}$ crystal has cubic symmetry with space-group $O_h^{10}(Ia3d)$ and eight formula units per unit cell.[24,25] The Y^{3+} ions occupy six crystallographically equivalent but orientationally inequivalent sites with dodecahedral point symmetry (D_2 point group). As the optically active ions are doped into the garnet, they normally substitute for the Y^{3+} ions and experience the same D_2 symmetry. The site symmetry is shown schematically in Fig. 1 where x, y, and z are labels for the local orthogonal C_2 axes for the D_2 symmetry of site 1.[26] The D_2 point group symmetry has four one-dimensional irreducible representations Γ_1, Γ_2, Γ_3, and Γ_4, and the transition dipoles necessarily lie along either x, y, or z, depending on the electronic states, according to the selection rules for electric and magnetic dipole transitions in D_2 symmetry.[27] Since the local x,y,z axes of the six sites are oriented differently from each other, the six sets of dipoles (arising from the six sets of Y^{3+} sites) will also be oriented differently, even though the sites are crystallographically equivalent. In a coherent transient application, if the electric field vector of the light beam makes unequal angles with each of the six classes of dipoles, unequal transition intensities will result for different sites and consequently different nutation frequencies Ω_i [Eq. (1)]. From the general solution given in Table I, we find that when the polarization is along [111], [001], and their equivalents, the electric field vector $\vec{E}$ (light polarization) will have the same angles relative to a group of the transition dipoles, resulting in identical Rabi frequencies and contributions to the transition intensity, while the remaining dipoles are perpendicular to $\vec{E}_0$ and are not excited. Details are given in Sec. VI where the orientation of the dipoles for this transition is deduced.

The 0.1% Tm^{3+}:$Y_3Al_5O_{12}$ crystal was grown at Scientific Materials Corp. and cut and polished with (110) and (111) faces, 3.6 mm along the $[1\bar{1}0]$ direction and 5.3 mm along the [111] direction. The crystal was immersed in liquid helium at 1.4 K. The $^3H_6(1) \leftrightarrow {}^3H_4(1)$ transition (793.156 nm) has an inhomogeneous linewidth of 20 GHz and a peak absorption coefficient of 1.5 cm^{-1}. The total absorption strength $\int \alpha d\sigma$ is 1.6 cm^{-2}.

An argon ion laser pumped single-frequency cw Ti:sapphire laser (Coherent 899-21) with 1 MHz frequency jitter was used in this experiment. A liquid crystal laser power controller (Cambridge LPC) was used to maintain laser power on the crystal constant within 1% in different experimental conditions. Two acousto-optic modulators in tandem were used to generate square optical pulses with ~ 20 μs duration. The laser was focused into the modulators to produce pulses with a fast rise time of 50 ns. Because of the long lifetime of the intermediate $^3F_4$ metastable level, the experiment was carried out at a 20 Hz repetition rate to allow the excited state population to relax back to the ground state between pulses. An aperture was used to clean up the edge of the collimated laser beam after the acousto-optic modulators. The laser beam passed through a $\lambda/2$ retarder and then a Glan-Taylor polarizing prism that was used to control the laser polarization. The polarizer was rotated to the desired polarization direction and then the $\lambda/2$ retarder was rotated to achieve maximum light output through the polarizer. An $f = 7.5$ cm lens was used to focus the laser onto the crystal with an $\omega_0 = 14$ μm waist radius. The crystal was oriented so that the laser propagated along either the $[1\bar{1}0]$ or [111] direction. The transmitted light was measured by an EG&G FND-100 photodiode and averaged using a Tektronix TDS620A digitizing oscilloscope.

V. OBSERVED POLARIZATION DEPENDENCE OF OPTICAL NUTATION

As expected from Table I, the optical nutation signal for light polarized along [111] and [001] exhibits single-Rabi-frequency behavior. The optical nutation signal $I_{\langle 111 \rangle}$ was recorded as a function of laser intensity to verify that the signal was nutation, not some artifact of the experimental setup. The laser intensity dependence of the signals and frequency of the nutation are shown in Fig. 2. The laser intensity was adjusted from 1.1 W/cm^2 to 2.8×10^3 W/cm^2 at the focus. As expected, the nutation frequencies were propor-

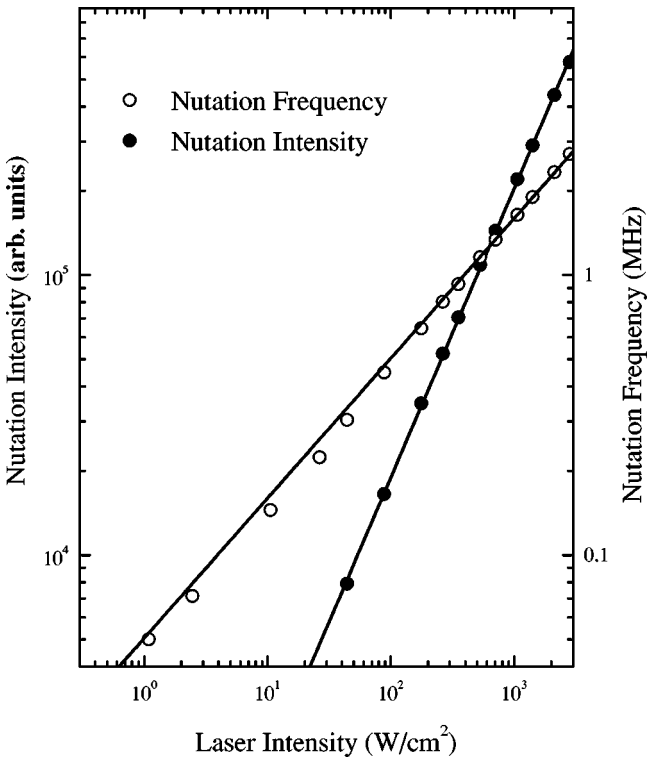

FIG. 2. Laser intensity dependence of the nutation signal and nutation frequency. The incident laser intensity was varied over 3.5 decades. The signal changes linearly with the intensity while the frequency changes with the square root of the intensity.

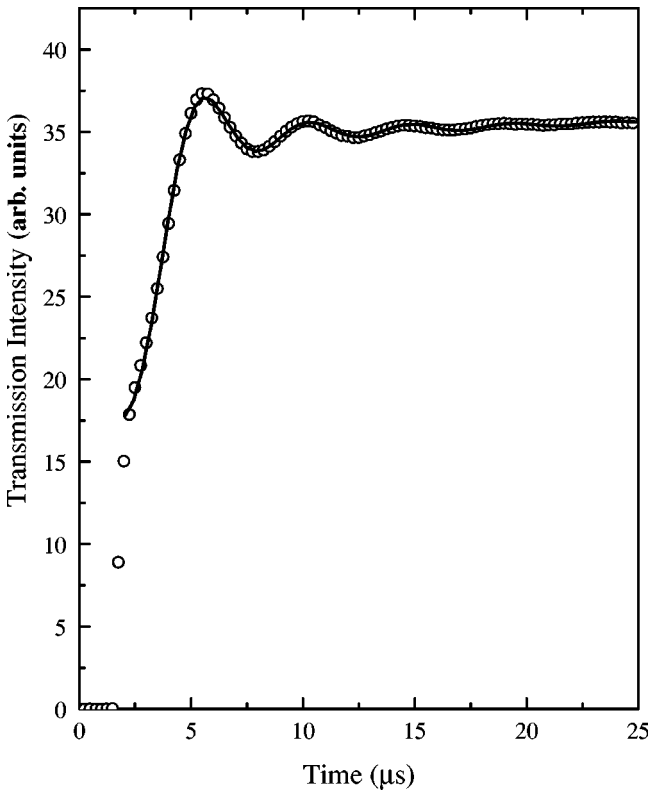

FIG. 3. Observed nutation signal of the $^3H_6(1) \leftrightarrow {}^3H_4(1)$ transition of 0.1% Tm^{3+}:$Y_3Al_5O_{12}$ for a laser propagating along the $[1\bar{1}0]$ direction and polarized along [111]. The incident power was $\sim$26.3 W/cm^2. The solid line through the data was a simulation using Eq. (1).

tional to the laser electric field and the nutation signals were proportional to the laser intensity, confirming the first-order approximation of Eqs. (1) and (2). In Fig. 3, we present the nutation of this transition with the laser intensity at 26.3 W/cm^2 along with a fit of the signal to Eq. (1) (solid line), and we can see that the simple model describes the nutation quite well. In Fig. 4, we present the nutation signals observed in this crystal at the light intensity of 1.76×10^3 W/cm^2, with the light propagating along the $[1\bar{1}0]$ direction and the light polarization rotated in the plane perpendicular to it from [110] to [001] in steps of $\sim 5°$ as illustrated in Fig. 1. Especially interesting are the directions of [111] (C_3 axis) and [001] (C_4 axis) since those are the directions where simple single-dipole nutation behavior is expected and observed. As we can see from this graph, even a misalignment of a few degrees can make a dramatic difference in the temporal behavior of the nutation signal. The nutation signals are all calculated in Sec. VI with only the parameters obtained from fitting the special [111] and [001] direction signals to Eq. (1).

The optical nutation for light propagating with $\vec{k}$ along the [111] direction was also studied. As $\vec{E}_0$ was rotated, the nutation signal was recorded. None of the measured nutations has the special single-Rabi-frequency behavior since $\vec{E}_0$ will not have identical projections on all the dipoles for any $\vec{E}_0$ direction in the (111) plane. We also observed, as expected, that the nutation traces repeated themselves as $\vec{E}_0$ was rotated by 60°, due to the threefold symmetry around the [111] axis.

VI. ORIENTATION AND MAGNITUDE OF TRANSITION DIPOLES

For the local D_2 symmetry of the Tm^{3+} ions, we expect the transition dipole for the $^3H_6(1)$ to $^3H_4(1)$ transition to be along the x, y, or z axis of local symmetry as shown in Fig. 1. In our convention, x and y are along the $\langle 110 \rangle$ axes of the crystal, while z is along the $\langle 001 \rangle$ axis. First, consider the case where this dipole is along one of the $\langle 110 \rangle$ directions, e.g., the y axis of site 1 in Fig. 1. When the electric field vector of the laser is along any of the threefold symmetry axes ([111] and its equivalents), the laser induces transitions at identical Rabi frequencies for three of the six sites (1, 3, and 5 in Fig. 1) and has no interaction with the remaining three. When the electric field vector of the laser is along any of the fourfold symmetry axes ([001] and its equivalents), the laser induces transitions at identical Rabi frequencies for four of the six sites (3, 4, 5, and 6 in Fig. 1) and has no interaction with the remaining two (1 and 2 in Fig. 1). We expect the Rabi frequencies to be different in these two cases. The Rabi frequency with $\vec{E}_0 \| [111]$ is expected to be faster than that of $\vec{E}_0 \| [001]$ by a ratio of $\cos 35.3°/\cos 45° \equiv \sqrt{4/3}$. Second, consider the case that this dipole is along one of the $\langle 001 \rangle$ directions, e.g., the z axis of site 1 in Fig. 1. When the electric field vector of the laser is along any of the threefold symmetry axes ([111] and its equivalents), the laser induces transitions at all six sites with identical Rabi frequencies. When the electric field vector of the laser is along any of the fourfold symmetry axes ([001] and its equiva-

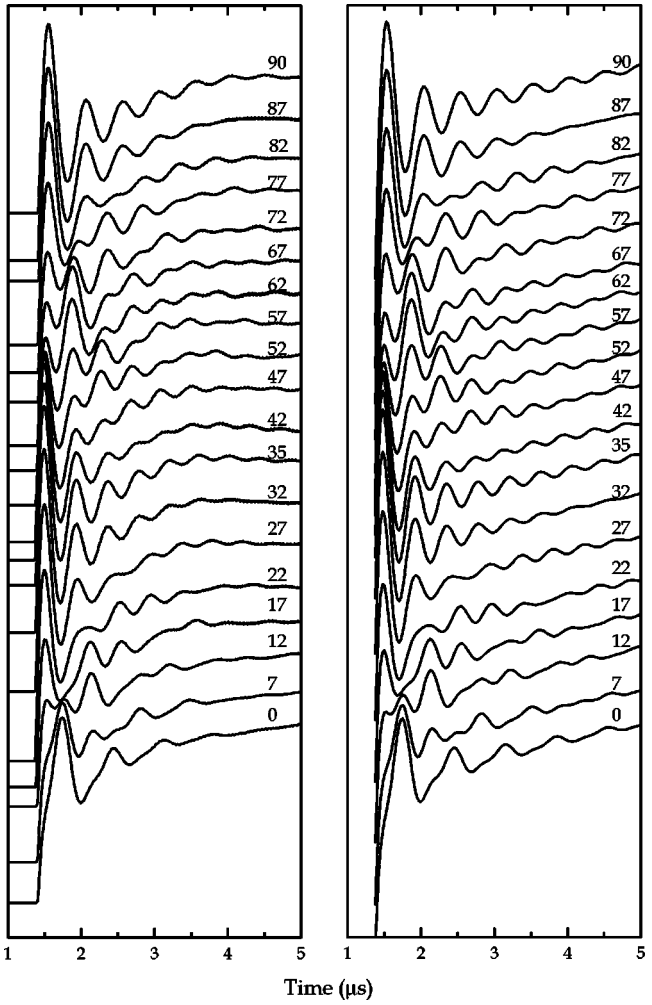

FIG. 4. On the left side are the observed optical nutation signals for the ${}^3H_6(1)\leftrightarrow{}^3H_4(1)$ transition of 0.1% Tm^{3+}:$Y_3Al_5O_{12}$ with the laser propagating along the $[1\bar{1}0]$ direction. The laser intensity on the crystal was 1.76×10^3 W/cm^2. The number above each trace is the angle α between $\vec{E}_0$ and [110]. On the right side are the calculated nutation curves for the same angles according to Eq. (2). The calculation used experimental parameters fitted only for the two directions $\vec{E}_0\|[111]$ ($\alpha=35.3°$) and $\vec{E}_0\|[001]$ ($\alpha=90°$). All other nutation signals were calculated according to Eq. (6) without further fitting.

lents), the laser induces transitions at identical Rabi frequencies for two of the six sites (1 and 2 in Fig. 1) and has no interaction with the remaining four sites. We again expect the Rabi frequencies to be different in these two cases and the Rabi frequency with $\vec{E}_0\|[001]$ is expected to be faster than that of $\vec{E}_0\|[111]$ by a ratio of $1/\cos 54.7°\equiv\sqrt{3}$.

As shown in Fig. 4, for the 35.3° ([111]) nutation signal, it is quite obvious that there is only one Rabi frequency. The same can be said about the nutation signal at $\alpha=90°$ ([001]). From a fit of Eq. (1) to the nutation data taken in the directions of [111] and [001], we found that the Rabi frequency is 2.34 MHz along [111] and 2.05 MHz along [001]. The ratio between the two frequencies is 1.165, very close to the expected value of $\sqrt{4/3}=1.155$ when the transition dipole is along the $\langle110\rangle$ direction. This implies that the transition dipole is along the $\langle110\rangle$ direction; and for the same laser intensity, the expected nutation Rabi frequency is $\sim$2.91 MHz if $\vec{p}\|\vec{E}_0$.

With the knowledge of the direction of the dipole, we can calculate the expected nutation signal due to all sites participating in the transition for all polarization directions in our experimental geometry. If the transition dipole for site 1 is along [110] in Fig. 1 (similar arguments follow if it is along $[1\bar{1}0]$), when the polarization is rotated in the $(1\bar{1}0)$ plane, there is a contribution to the nutation from site 1, site 2 does not participate in the transition, site 3 and site 5 contribute equally, and site 4 and site 6 contribute equally. If we call the angle the polarization makes with the [110] direction α, then we have

$$\Omega_1=\Omega_0\cos\alpha, \tag{3}$$

$$\Omega_3\equiv\Omega_5=\Omega_0(\cos\alpha/2+\sin\alpha/\sqrt{2}), \tag{4}$$

$$\Omega_4\equiv\Omega_6=\Omega_0|\cos\alpha/2-\sin\alpha/\sqrt{2}|, \tag{5}$$

where Ω_1 is due to site 1, $\Omega_3\equiv\Omega_5$ are due to sites 3 and 5, $\Omega_4\equiv\Omega_6$ are due to sites 4 and 6, and Ω_0 denotes the Rabi frequency when $\vec{p}\|\vec{E}_0$. The total nutation signal is a combination of the three according to Eq. (2) so that

$$S\propto\text{const}+\Omega_1^2\frac{J_1(\Omega_1 t)}{\Omega_1 t}+2\Omega_3^2\frac{J_1(\Omega_3 t)}{\Omega_3 t}+2\Omega_4^2\frac{J_1(\Omega_4 t)}{\Omega_4 t}. \tag{6}$$

From earlier discussions, we know the nutation Rabi frequency should be 2.91 MHz when $\vec{E}_0\|\vec{p}$ in our conditions. This value was used to calculate the nutation signals for $\vec{E}_0$ polarized along all of the directions in Fig. 4. As shown in Fig. 4, there is very good agreement between the experiment and the simulation, confirming our explanation of the complicated nutation behavior for $\vec{E}_0$ along an arbitrary direction. In the following calculation of the dipole moment and thus the oscillator strength, we use the standard Lorentz-Lorenz local field correction for the field interacting with the dipole. The conversion is $I=(c/8\pi)[9n/(n^2+2)^2]|E_0|^2$. $n=1.822$ at 793 nm for YAG. Thus, $9n/(n^2+2)^2=0.58$. For the laser intensity (1.76×10^3 W/cm^2) and the nutation frequency (2.91 MHz), we calculate E_0 to be 3.83 statvolts/cm and the dipole moment to be 5.03×10^{-21} esu cm. This corresponds to an oscillator strength of 8.7×10^{-8}. From our absorption experiment, this transition has $\int\alpha d\sigma=1.6$ cm^{-2}. The 0.1% Tm^{3+} doping corresponds to 1.39×10^{19} ions per cm^3. The calculated oscillator strength is 7.6×10^{-8} from the absorption spectrum with the same local field correction. The results from the two independent measurements are in very good agreement. In cases when the number density is not well determined, optical nutation provides an independent way to measure the oscillator strength. It is also useful to resolve site occupancy issues.[15]

VII. SUMMARY

In conclusion, for all possible combinations of space group and point groups, a combination of propagation and polarization directions exists that provides single-Rabi-frequency behavior for coherent light-matter interactions.

This provides optimum coupling, signal strength, and transient response for spectroscopy and for device applications. In particular, this eliminates the deleterious effects of multiple-Rabi-frequency interference, allowing use of low-symmetry materials with otherwise ideal properties that would have been rejected until now on account of this site interference.

Single-Rabi-frequency optical nutation, illustrating the efficacy of this strategy, has been observed for $Pr^{3+}:Y_2SiO_5$, Tm^{3+}:YAG, and the $Er^{3+}\,^4I_{15/2}(1) \leftrightarrow {}^4I_{13/2}(1)$ transition in $Er^{3+}:YAlO_3$, $Er^{3+}:LiNbO_3$, $Er^{3+}:CaWO_4$, $Er^{3+}:SrWO_4$, $Er^{3+}:Y_2O_3$, $Er^{3+}:Y_3Al_5O_{12}$, and $Er^{3+}:Y_2SiO_5$.

Detailed results were presented for $Tm^{3+}:Y_3Al_5O_{12}$. Two special light polarization directions $\langle 111\rangle$ and $\langle 001\rangle$ were found where the transition dipoles of all sites excited by the light field project equally onto the field vector. The optical nutation signals exhibited the desired cooperative properties under coherent illumination. For other polarizations, complicated irregular optical nutation signals were observed due to the interference of the different frequency components from several sites in the crystal, which was quantitatively explained. The transition dipole moment has been measured from both optical nutation and optical absorption and the results agree to within 15%. The dipole orientation is also determined from the optical nutation measurement with different light polarizations and is oriented along the $\langle 110\rangle$ direction. Determination of site occupancy in multisite materials was also discussed.

ACKNOWLEDGMENTS

Research at Montana State University was supported in part by Scientific Materials Corporation, Bozeman, Montana, AFOSR (Grant Nos. F49620-98-1-0171 and F49620-94-1-0465), NASA EPSCoR, and NSF EPSCoR.

[1] T. W. Mossberg, Opt. Lett. **7**, 77 (1982).
[2] W. R. Babbit and T. W. Mossberg, Appl. Opt. **25**, 962 (1986).
[3] A. Rebane, R. Kaarli, P. Saari, A. Anijdg, and K. Timpmann, Opt. Commun. **47**, 173 (1983).
[4] P. Saari, R. Kaarli, and A. Rebane, J. Opt. Soc. Am. B **3**, 527 (1986).
[5] *International Tables for Crystallography*, 4th revised ed., edited by T. Hahn (Kluwer Academic Publishers, Dordrecht, 1996), Vol. A.
[6] L. Allen and J. H. Eberly, *Optical Resonance and Two-Level Atoms* (Dover, New York, 1987).
[7] T. L. Harris, Y. Sun, R. L. Cone, R. M. Macfarlance, and R. W. Equall, Opt. Lett. **23**, 636 (1998).
[8] G. B. Hocker and C. L. Tang, Phys. Rev. Lett. **21**, 591 (1968).
[9] R. G. Brewer and R. L. Shoemaker, Phys. Rev. Lett. **27**, 631 (1971).
[10] R. G. Brewer and A. Z. Genack, Phys. Rev. Lett. **36**, 959 (1976).
[11] B. W. Shore, Phys. Rev. A **17**, 1739 (1978).
[12] C. Delsart and J. C. Keller, J. Phys. B **13**, 241 (1980).
[13] A. Kastberg, P. Villemoes, A. Arnesen, F. Heijkenskjöld, and A. Langereis, Opt. Commun. **101**, 25 (1993).
[14] R. L. Shoemaker and E. W. Van Stryland, J. Chem. Phys. **64**, 1733 (1976).
[15] Y. Sun, F. Könz, R. L. Cone, and R. W. Equall, Bull. Am. Phys. Soc. **44**, 1937 (1999).
[16] R. L. Shoemaker, in *Laser and Coherence Spectroscopy*, edited by J. I. Steinfeld (Plenum Press, New York, 1978), Chap. 3.
[17] J. B. Gruber, M. E. Hills, R. M. Macfarlane, C. A. Morrison, G. A. Turner, G. J. Quarles, G. J. Kintz, and L. Esterowitz, Phys. Rev. B **40**, 9464 (1989).
[18] C. Tiseanu, A. Lupei, and V. Lupei, J. Phys.: Condens. Matter **7**, 8477 (1995).
[19] R. M. Macfarlane, Opt. Lett. **18**, 1958 (1993).
[20] H. Lin, T. Wang, and T. W. Mossberg, Opt. Lett. **20**, 1658 (1995).
[21] K. D. Merkel and W. R. Babbit, Opt. Lett. **21**, 71 (1996).
[22] K. D. Merkel and W. R. Babbit, Opt. Lett. **23**, 528 (1998).
[23] K. D. Merkel and W. R. Babbit, Opt. Lett. **24**, 172 (1999).
[24] S. Geller and E. A. Wood, Acta Crystallogr. **9**, 563 (1956).
[25] S. Geller, Z. Kristallogr. **125**, 1 (1967).
[26] D. Boakes, G. Garton, D. Ryan, and W. P. Wolf, Proc. Phys. Soc. London **74**, 663 (1959); J. F. Dillon, Jr., and L. R. Walker, Phys. Rev. **124**, 1401 (1961); W. P. Wolf, M. Ball, M. T. Hutchings, M. J. M. Leask, and A. F. G. Wyatt, J. Phys. Soc. Jpn. **17**, Suppl. B-I, 443 (1962).
[27] G. F. Koster, J. O. Dimmock, R. G. Wheeler, and H. Statz, *Properties of the 32 Point Groups* (MIT Press, Cambridge, 1963).